의학박사 학위논문

비임상시험에서 간기능 및 간섬유화 평가를 위한 가도제테이트 역동조영증강 자기공명영상 및 초음파횡파탄성영상 기법 확립

Gadoxetate dynamic contrast-enhanced MRI and ultrasonographic shear wave elastography for evaluation of liver function and fibrosis in preclinical trial

울 산 대 학 교 대 학 원

의 학 과

허 지 미

비임상시험에서 간기능 및 간섬유화 평가를 위한 가도제테이트 역동조영증강 자기공명영상 및 초음파횡파탄성영상 기법 확립

지 도 교 수　　김 경 원

이 논문을 의학박사 학위 논문으로 제출함

2018년　2월

울 산 대 학 교　대 학 원

의　　학　　과

허　지　미

허지미의 의학박사 학위 논문을 인준함

심사위원	김정곤	인
심사위원	김경원	인
심사위원	우동철	인
심사위원	김형중	인
심사위원	서니은	인

울 산 대 학 교 대 학 원

2018년 2월

ABSTRACT

Objective:

Non-invasive imaging evaluation of the liver fibrosis and liver function has huge emphasis currently when huge efforts have garnered to develop new drug for liver fibrosis and chronic liver disease. Shear wave elastography (SWE) and gadexetate-enhanced DCE-MRI have been utilized in clinical researches, however rarely used in preclinical trial due to lack of validation. In this regard, we aim to validate the SWE and gadoxetate-enhanced DCE-MRI in an animal model of liver fibrosis.

Methods:

Thirty-one SD rats were randomly assigned into three groups (high-dose, low-dose, and control). The liver fibrosis was induced in SD rats by administration of thioacetamide intraperitoneally for 8 weeks: 200mg/kg for high-dose group and 150 mg/kg for low-dose group. At the end of thioacetamide administration period, we performed SWE twice with two days interval and performed gadoxetate-enhanced DCE-MRI. Liver stiffness in kPa was measured in the SWE. Five DCE-MRI indices (RLE-3, RLE-15, iAUC-3, iAUC-15, Emax) were calculated using MATLAB-based software. The correlation between these imaging parameters and histopathologic results and indocyanine green (ICG) R15 test results were calculated. The diagnostic performance to diagnose liver fibrosis was also evaluated.

Results:

On histopathology, animal model was successful in that the collagen areas was highest in high-dose group (24.86 ± 4.55), followed by low-dose group (16.01 ± 3.25), and control

group (6.27 ± 2.10). The correlation between the histopathologic collagen area and imaging parameters was similarly high in iAUC-15, iAUC-3, and RLE-3 (-0.78 to -0.81), but low in RLE-15 (-0.51) and liver stiffness in kPa (-0.59). The correlation coefficients between MRI indices and liver function on ICG-R15 was highest in iAUC-15 (-0.65) followed by iAUC-3 (-0.63), RLE-3 (-0.62), Emax (-0.58), and RLE-15 (-0.56). In the ROC analysis to diagnose liver fibrosis (i.e., high-dose group and low-dose group), the diagnostic accuracy of RLE-3, iAUC-3, iAUC-15, and Emax were 100% (AUROC 1.000) with complete differentiation between the liver fibrosis groups and control group. In contrast, the diagnostic value of the RLE-15 was significantly lower than the other MRI indices (AUROC 0.777)

Conclusions:

Theoretically, the ultrasonographic SWE reflects liver fibrosis and the gadoxetate-enhanced DCE-MRI reflects liver function. In our study using the animal liver fibrosis model, the ultrasonographic SWE and gadoxetate-enhanced DCE-MRI are quite feasible to evaluate both histopathologic liver fibrosis and physiologic liver function in non-invasive manner in preclinical trial.

Keywords: Gadoxetate, Dynamic contrast-enhanced, Magnetic resonance imaging, Shear wave elastography, Validation

차 례

표 목차

그림목차

INTRODUCTION

There have been huge efforts to develop new drug for liver fibrosis and chronic hepatitis in the last several decades. Accordingly, drug efficacy test in the preclinical trial as well as clinical trial has been continuous increasing in the field of anti-fibrotic agents for the chronic liver disease. Non-invasive monitoring tool is very useful to assess the treatment response to the new drug candidate (1).

Liver ultrasonographic elastography is an emerging technique for evaluating liver cirrhosis by measuring the liver stiffness using shear wave speed in the liver tissue. Transient elastography (TE) is the most widely used technique as a first commercialized tool (Fibroscan; Echosens, Paris, France) (2), however, TE has several technical limitations such as ascites, obesity, narrow intercostal space, etc (3). Shear wave elastography (SWE) is a recently developed technique that assesses the tissue mechanical properties monitoring the speed of shear wave generating from tissue deformation produced by the acoustic radiation force (4). The SWE is incorporated with gray-scale images enabling overlay of the color elastogram map (3). Currently, SWE is in the clinical validation stage which evaluate whether SWE biomarkers can reflect pathologic process and clinical outcome and whether SWE can provide results in reproducible manner (5). Especially, to use SWE as a quantitative biomarker for new drug development or treatment response assessment, ensuring repeatability in measurement is very important. Therefore, the quantitative imaging biomarker alliance (QIBA) has organized a technical committee and proceeded the validation process (6).

Gadolinium ethoxybenzyl diethylenetriaminepentaacetic acid (Gd-EOB-DTPA; hereafter referred to as gadoxetate) is a dual-function contrast agent for magnetic resonance image (MRI). At the vascular phase, gadoxetate acts as an extracellular contrast agent to

evaluate hemodynamic change or vascularity. At the later phase, gadoxetate acts as a hepatocyte-specific contrast agent to enhance hepatocytes (7, 8). The characteristics of gadexetate as a hepatocyte-specific contrast agent enable to evaluate the liver function (9, 10).

Dynamic contrast-enhanced MRI (DCE-MRI) allows characterization of functional aspects of biologic tissue by using both the temporal information and the spatial information provided by MRI (11, 12). Liver function is generally estimated by indocyanine green (ICG) test such as ICG-R15 or ICG clearance test. In the liver tissue, gadoxetate and ICG use the same receptors such as OATP and MRP, theoretically, the DCE-MRI results can reflect the ICG test.

These liver fibrosis and liver function imaging have been largely studied in the clinical research. However, still, preclinical trial rarely uses these imaging modalities. One of the main reasons is a lack of supporting evidence in preclinical trial. In this regard, utilization of SWE technique and gadexetate-enhanced DCE-MRI in the preclinical trial might be very powerful tool, as long as the technical feasibility is proven and the repeatability is ensured. From this perspective, we performed an animal study to evaluate the biomarker validation in the rat liver fibrosis model.

Materials and Methods

Animal model

All experiments associated with this study were approved by our institutional animal care and use committee. A drug-induced chronic liver injury model is adopted to generate liver fibrosis. All SD rats (male, 8 weeks old, 270-280 g weight) were obtained from Orient Bio (Seoul, Korea) and were maintained under specific pathogen-free conditions.

In order to model drug-induced liver injury, we used thioacetamide (TAA, Sigma-Aldrich CO., St Louis, MO, USA) which is a hepatotoxic agent causing centrilobular necrosis (13). To minimize any potential bias from the researcher's selection, thirty four rats were randomly assigned to one of three groups by using a computerized random number generator (https://randomizer.org). The assignment resulted in 8 rats in control group, 11 rats in low-dose group, and 15 rats in high-dose group.

For eight weeks, intermittent intraperitoneal injection (three times per week) of TAA or saline was performed: TAA 200mg/kg for high-dose group, TAA 150mg/kg for low-dose group, and saline for control group. The dose of TAA was determined by our preliminary experiment (results not shown) using 100 mg/kg, 150mg/kg, 200mg/kg, and 250mg/kg of TAA. In which, the 100 mg/kg dose did not induce liver fibrosis consistently and 250 mg/kg dose resulted in death during TAA medication period. Therefore, we decided to use 150 mg/kg and 200 mg/kg for this experiment.

After eight weeks of TAA medication, imaging examinations including SWE and MRI were performed.

Shear Wave Elastography

Two-dimensional SWE measurements were acquired with an Aplio 500 Platinum

ultrasound machine (Toshiba Medical Systems Corporation, Tokyo, Japan) using a linear probe (PLT-1005BT transducer (7.0–14.0 MHz). Measurements were acquired by a single operator (Y.C.C), a radiographer who has 5 years of experience in animal CT and ultrasonographic imaging. The operator received hard training in 2D SWE before study commencement.

The rats fasted for 4 hours before testing. Under anesthesia with isoflurane, the rats were positioned in the supine position with the both anterior limbs abducted. After shaving the upper abdomen, the transducer was gently applied with a large amount of sonographic jelly to achieve a good acoustic window while avoiding artifacts of stiffness radiating from the contact area and hand motion. Measurements were taken from the left hepatic lobe. The operator measured the SWE using at the similar depth of 1cm from the liver surface in all animals.

Measurements were obtained in the liver parenchyma away from vascular or biliary structures. The measurement ROIs with 0.3 cm diameter were placed in areas of greatest shear wave uniformity which showed relatively homogeneous color on the speed map (Figure 1). Measurements were performed 8-10 times per animal and 3-4 times per single-shot acquisition. Measurement results were recorded in kilopascal (kPa). Among the measurements, we selected the four measurements in the middle, according to the WUFUMB guidelines.

In all rats, SWE examinations were performed in two measurement sessions with 3-day interval to evaluate test-retest repeatability of SWE.

Figure 1. Measurement of shear wave elastography. Regions-of-interest (ROIs) are positioned in an area with homogenous color on elasticity map (a) and speed map (b).

(a) Liver stiffness map which show the distribution of liver stiffness in kPa in the liver.

(b) Speed map which show the distribution of shear wave velocities in the liver.

(a)

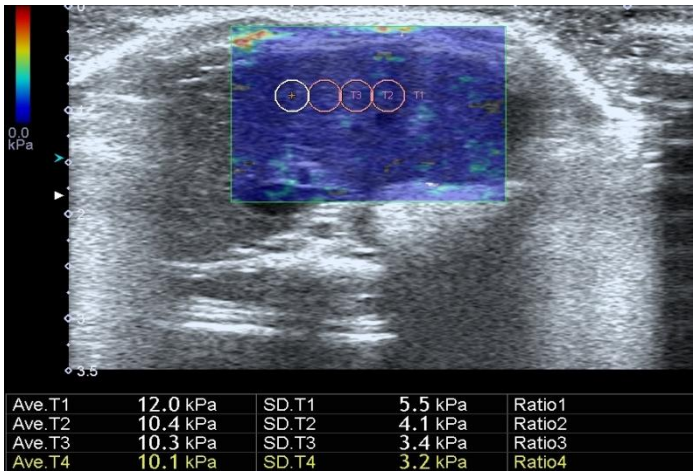

(b)

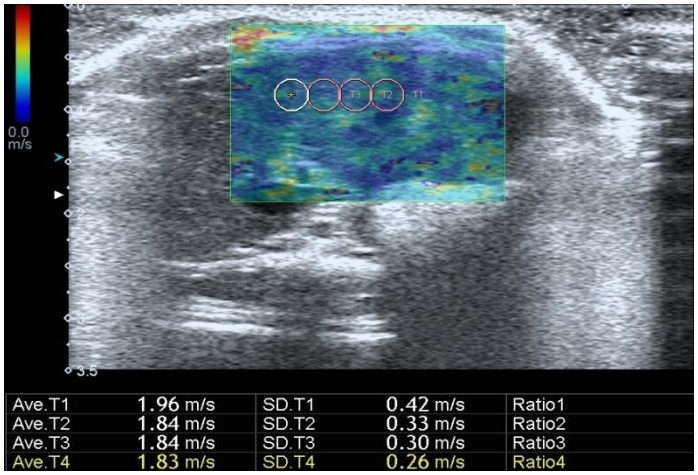

MRI acquisition

A 3-T MR scanner (Magnetom Skyra; Siemens Healthcare, Erlangen, Germany) with a 16-channel hand/wrist coil was used. The rats were anesthetized during the imaging session with 1.3-1.5 % isoflurane/air mixture. DCE-MRI including T1 map was acquired using CAIPIRINHA-VIBE sequence, which was proven as a motion-insensitive and fast scanning method. CAIPIRINHA-VIBE was performed with the following parameters: TR/TE 4.3/1.5 ms; flip angle 25°; matrix size 128x128; and an acceleration factor of 4 (2 each in the phase- and partition-encoding directions) with a reordering shift of 1. The scan coverage of this sequence was 78 mm (52 slices×1.5 mm thickness) and the field of view was 100 x 100 mm, which was sufficient for covering the entire liver in all the rats.

As to the DCE-MRI scanning, T1 map was generated with variable flip-angle technique (α=2°, 8°, 15°, 22°, 29°) without contrast agent injection. During dynamic scanning, five-phase baseline acquisitions were performed before contrast agent injection. When the sixth phase acquisition was started, 0.05 mmol/kg of body weight of gadoxetic acid (Eovist or Primovist, Bayer Healthcare, Berlin, Germany) was injected at a rate of 2 mL/s followed by a saline chase of 0.3 mL at the same injection rate. Then, a dynamic series was repeatedly every 3.6 seconds for 3 minutes and then every 60 seconds for 30 minutes.

DCE-MRI analysis

We developed a comprehensive software, Asan J, combining the Image J (NIH, Bethesda, Maryland, USA) and the MATLAB (The MathWorks, Natick, MA, USA). Our software has modules to evaluate liver function using the signal intensity (SI) measured on MRI.

The SI was measured on a pixel-by-pixel basis using the Asan J software. An

experienced radiologist (J. H.) with more than 9 years of experience measured the SI of the rat liver at three different regions of interest (ROIs) in the liver parenchyma, avoiding enhancement of vessels and bile structures. Another experienced radiologist (K.W.K.) with more than 12 years of experience double-checked the ROIs. The mean SI of each ROI was recorded and used for analysis.

Based on the SI, the relative liver enhancement (RLE) at 3 minutes (RLE-3) and 15 minutes (RLE-15) after contrast agent injection were calculated using the following formula (12, 14):

$$RLE = (SI_{Liver\text{-}enh} - SI_{Liver\text{-}unenh}) / SI_{Liver\text{-}unenh}$$

Initial area of under the curve (iAUC) until 3 minutes (iAUC-3) and until 15 minutes (iAUC-15) from contrast agent injection were calculated by integral at the time-enhancement curve (15). The maximum enhancement (Emax) was also acquired.

Histopathology

After the second ultrasonographic examination, the animals were euthanized in a carbon dioxide chamber. We performed en-bloc resection of the liver and sliced the liver at 5 mm intervals in a cross-sectional manner. The excised tissues were then fixed in 10% formalin, and paraffin blocks were made. For microscopic evaluation of the liver parenchyma, hematoxylin and eosin (H&E) staining was performed. To evaluate the extent of liver firbosis, the Masson's trichrome stain was performed with a commercially available kit (Sigma-Aldrich Korea, Seoul, Korea). In the Masson's trichrome stain, the cytoplasm and muscle fibers stain red whereas collagen displays blue coloration (16, 17).

The collagen areas were quantified using NIH-Image J software (NIH, Bethesda, MD) as following steps: (1) The three representative hot spots were determined at lower

magnification (x40); (2) Those areas were captured and digitized for morphometric analysis; (3) The collage areas were selected with the colorimetric threshold of the blue color. If the collage areas were not selected automatically by Image J, we adjusted the areas manually while referencing the H&E stain. The measurement values from those five hotspots were averaged and used for statistical analysis.

Indocyanine Green test

To evaluate the liver function, the ICG retention rate at 15 minutes (ICG-R15) test was performed, which is the most widely used method in the clinical practice (18). The ICG-R15 is the ratio between ICG concentration 15 minutes after injecting ICG (C-15) and initial concentration (C-0), calculating by the formula: ICG-R15 (%) = C-15/C-0 × 100.

The ICG (Daiichi Sankyo, Tokyo, JP) was dissolved in normal saline to a final concentration of 2.5 mg/mL. The right carotid artery was surgically exposed and cannulated for blood sampling. The ICG solution with concentration of 2.5 mg/Kg body weight was injected through the tail vein. Blood sample was obtained at 15 minutes after ICG injection and mixed with ethylenediaminetetraacetic acid (EDTA) 20 μl. The blood sample was then centrifuged to get plasma. The plasma sample was diluted with 1% bovine serum albumin (BSA) solution. The ICG concentration in the plasma sample was measured spectrophotometrically at 805 nm (i.e., C-15). The initial concentration (C-0) is calculated by estimating that 2.5 mg/Kg ICG in a rat with a plasma volume of 40 ml/kg body weight (19), yielding 16 mg/ml.

Statistical Analysis

The mean value and standard deviation (SD) were determined for all continuous

variables. For comparison of mean values of liver stiffness (kPa) on SWE between measurement sessions and across groups, repeated measures analysis of variance (RMANOVA) was used. Other quantitative values were compared between the three sequences by using one-way ANOVA with post hoc analysis of Tukey-Kramer method.

The correlation was calculated between continuous variables, the pearson correlation coefficient was used. The diagnostic accuracy to diagnose liver fibrosis including low-dose and high-dose group, was evaluated by receiver operating curve (ROC) and area under the ROC (AUROC). A p value < 0.05 was considered to indicate a statistically significant difference. MedCalc version 17.7.2 (MedCalc Software bvba, Ostend, Belgium) and IBM-SPSS Statistics for Windows, Version 21.0 (IBM Corp., Armonk, NY, USA) were used.

For calculation of test-retest repeatability of kPa, we used the statistical methods recommended by the Radiological Society of North America (RSNA) (https://www.rsna.org) methodological guides (20-22). Statistical analysis was performed using a web-calculator (available at http://datasharing.aim-aicro.com/reliability) which follows the most updated methodological guides. In addition, the test-retest repeatability was also evaluated using Bland–Altman plots with the mean relative difference and 95% limit of agreement (LOA) (23). Agreement between two measurements was visually assessed using Bland–Altman plots in which the relative differences were plotted against the average values of two size measurements. The 95% LOA is the range of the mean relative difference ± 1.96• SDs of the mean relative difference.

Results

Animal models

Among the 34 rats, 3 rats were died during the eight weeks of TAA injection. Finally, 8 rats in control group, 9 rats in low-dose group, and 14 rats in high-dose groups were included in this study. Signs of toxicity, such as ruffled fur, anorexia, cachexia, skin tenting, skin ulcerations, or toxic death (24), were not seen in any of the mice survived.

All rats in the control group showed normal histologic findings without fibrosis, inflammation, and steatosis. In all rats in low-dose group and high-dose group, H&E stain demonstrated damaged hepatic cells with apparent toxicity characterized by periportal hepatocytic vacoulation, centrilobular necrosis, heavy pigmentation around central veins, scattered inflammation, and giant cell transformation. On Masson's trichrome stain, liver fibrosis with abundant collagen deposit was successfully induced and the fibrous bands or septa originate from portal areas and extend into the hepatic parenchyma (Figure 2a).

The collagen areas in the liver histopathologic specimen was highest in high-dose group (24.86 ± 4.55), followed by low-dose group (16.01 ± 3.25), and control group (6.27 ± 2.10), as presented in Figure 2b. Post-hoc multiple comparison analysis revealed that all pairs of comparison showed statistically significant difference ($p<0.05$, Tukey-Kramer test for all pairwise comparisons).

The liver function test with ICG-R15 revealed that was highest in high-dose group (4.27 ± 2.07), followed by low-dose group (3.25 ± 1.39), and control group (1.05 ± 1.26), as presented in Figure 2c. Post-hoc multiple comparison analysis revealed that control group differ significantly with low-dose group and high-dose group, respectively, but there was no significant difference between low-dose group and high-dose group.

Shear Wave Elastography

The box-and-whisker plots of the liver stiffness in kPa measured from the 1st and 2nd sessions are presented in Figure 3a. The 2nd measurement session yielded more reliable results than the 1st measurement session in that the interquartile range (IQR), a measure of variability, was higher in the 1st measurement session than the 2nd measurement session. In addition, four outliers were present in the 1st measurement but not in the 2nd measurement. These results may suggest the training effect or learning-curve effect of the operator. Indeed, when we reviewed the four cases of outliers, there were areas of nonfilling and heterogeneity on the speed smart map, which are indicative of invalid shear wave characteristics (Figure 3b).

Liver stiffness differed significantly between groups ($p<0.001$, Between-subject effects of RMANOVA), however, did not differ between the 1st measurement (kPa-1st) and the 2nd measurement (kPa-2nd) ($p=0.122$, within-subject effects of RMANOVA). Post-hoc analysis showed that the liver stiffness differed between control group and liver fibrosis groups, but did not differ between low-dose group and high-dose group (Figure 3).

Figure 2. Histopathology of liver parenchyma

(a) Hematoxylin and eosin (HE) stain and Masson's trichrome (MT) stain at 200 × magnification)

(b) Comparison of collagen area (%) between groups

(c) Comparison of ICG-R15 (%) between groups

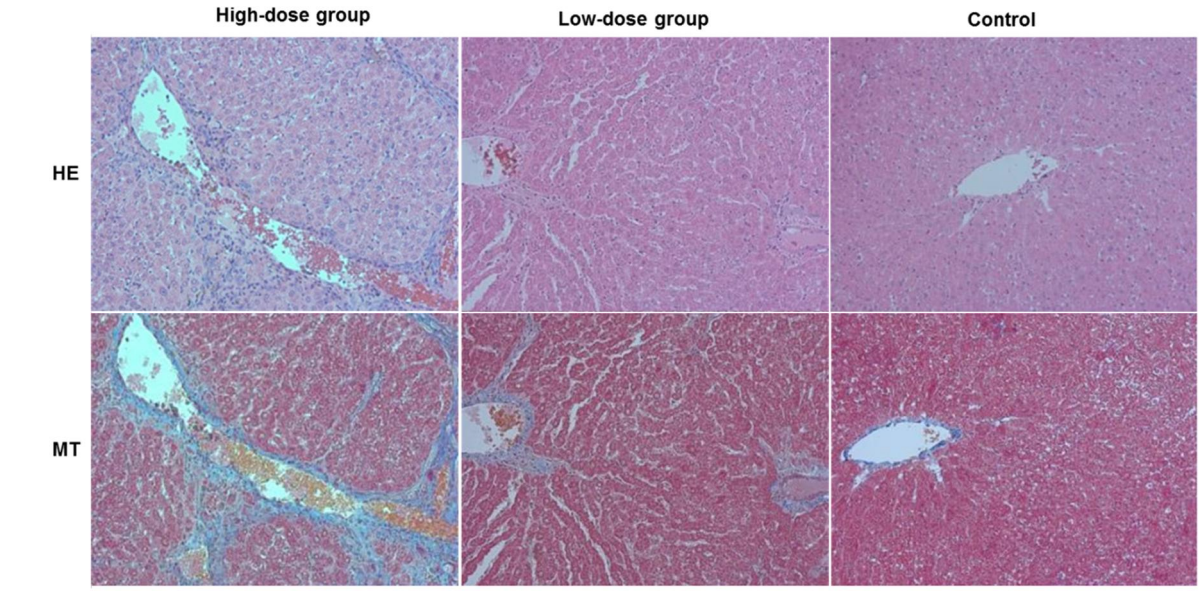

(a)

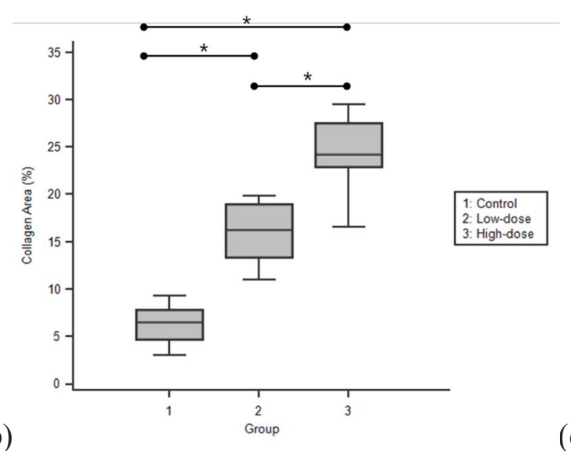

(b)

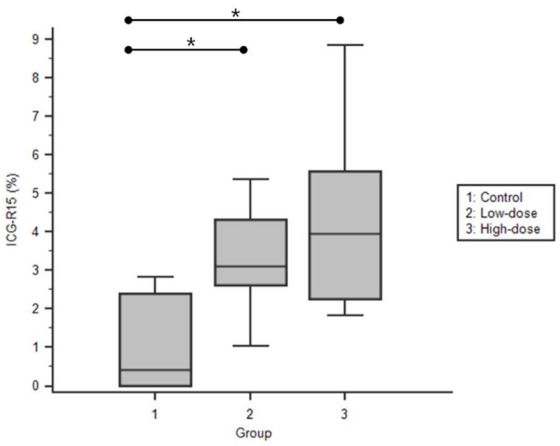

(c)

Figure 3. Liver stiffness measurement in each group.

(a) Box-and-whisker plots of the liver stiffness measured from the 1st and 2nd sessions. The outliers are presented as round dots in the 1st measurement sessions.

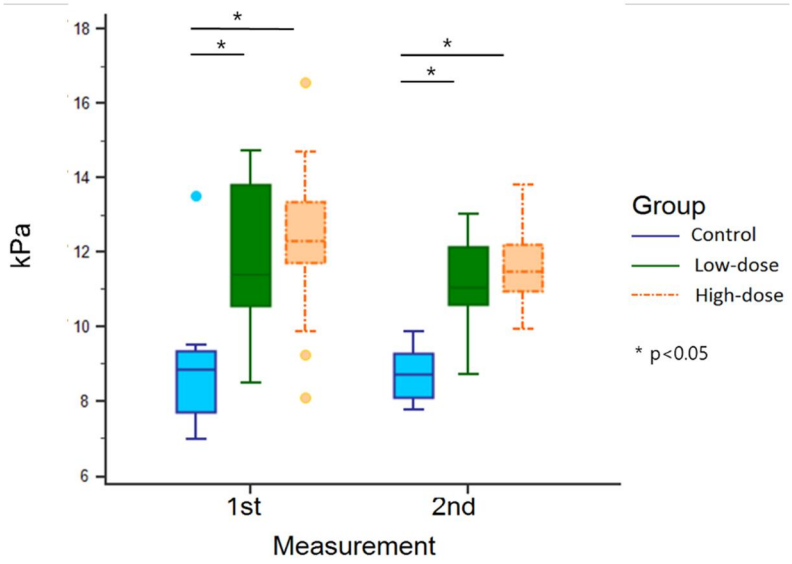

(b) Shear wave speed maps of control, low-dose, and high-dose group as well as outliers.

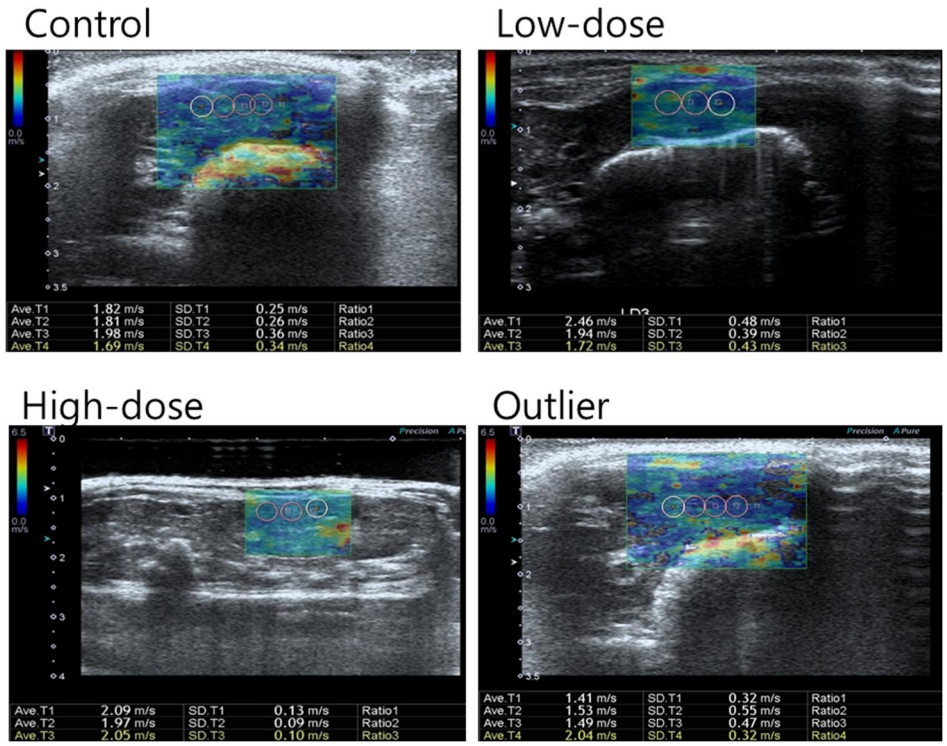

Liver stiffness differed significantly with the severity of liver fibrosis in that there was a significant positive correlation with liver stiffness (kPa-mean) and the collagen areas of liver specimen ($r = 0.59$, $p=.0.005$) (Figure 4).

The repeatability coefficient of liver stiffness over the 1st and 2nd measurement sessions were 3.75 kPa (95% confidence interval, 3.01 to 4.99 kPa; within-subject CV, 12.26 %). In the Bland-Altman analysis, the 95% LOA was -3.05 to 4.22 kPa. When the four outliers were removed, the repeatability coefficient decreased to 2.82 kPa (95% confidence interval, 2.24 to 3.85 kPa; within-subject CV, 9.29 %) and the Bland-Altman 95% LOA also decreased (-2.12 to 3.21 kPa) (Figure 5).

Figure 4. Correlation with liver stiffness (kPa) and the collagen area (%) of the liver specimen.

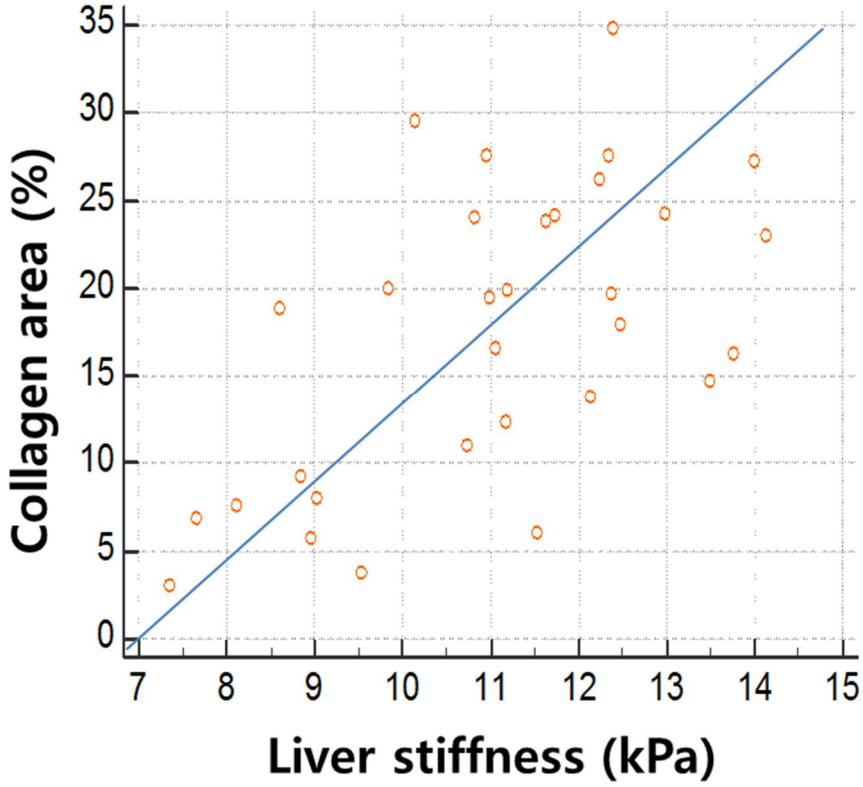

Figure 5. Bland-Altman plot to evaluate repeatability of liver stiffness measurement.

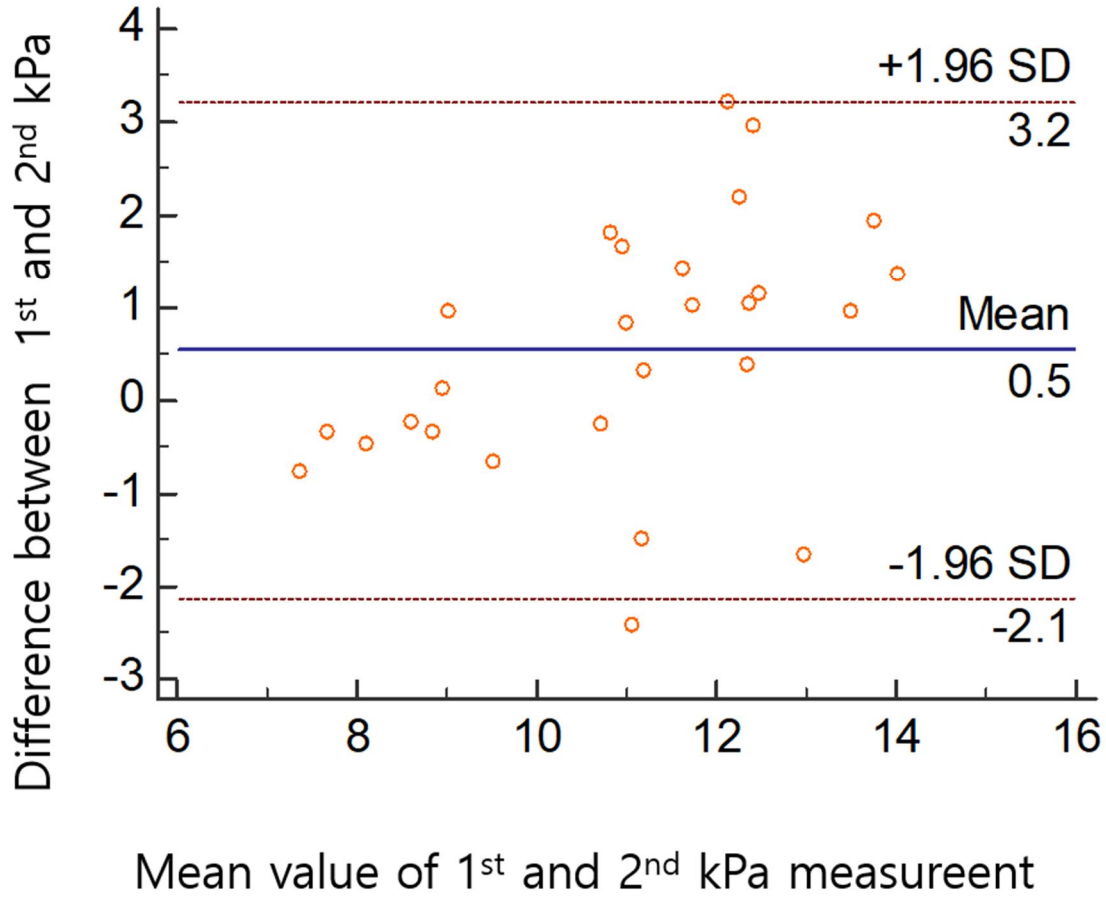

DCE-MRI

The SI of the liver in the gadoxetate-enhanced MRI is generally highest in the control group, followed by low-dose group and high-dose group (Figure 6). Indeed, all the MRI indices of liver function differed significantly between groups ($p<0.001$, One-way ANOVA), indicating that the low value of MRI indices is suggestive of liver fibrosis and low liver function. Post-hoc analysis revealed that the all MRI indices differed between control group and low-dose and between control group and high-dose group, except for RLE-15, as presented in Table 1. However, all MRI indices did not differ between low-dose group and high-dose group.

In the ROC analysis to diagnose liver fibrosis (i.e., high-dose group and low-dose group), the diagnostic accuracy of RLE-3, iAUC-3, iAUCR-15, and Emax were 100% (AUROC 1.000) with complete differentiation between the liver fibrosis groups and control group. In contrast, the diagnostic value of the RLE-15 was significantly lower than the other MRI indices (AUROC 0.777) (Figure 7).

There was negative correlation between all MRI indices and collagen area and between MRI indices and ICG-R15 (Table 2). The correlation coefficients between MRI indices and collagen area were similarly high in iAUC-15, iAUC-3, and RLE-3 (-0.78 to -0.81), but low in RLE-15 (-0.51). These results indicate that MRI indices reflect very well the histologic fibrosis severity.

The correlation coefficients between MRI indices and liver function on ICG-R15 was highest in iAUC-15 (-0.65) followed by iAUC-3 (-0.63), RLE-3 (-0.62), Emax (-0.58), and RLE-15 (-0.56) (Table 2). These results indicate that the MRI indices are relatively good in predicting liver function. Of these, iAUC-15 might be the best semi-quantitative parameter to evaluate both liver function and histopathologic liver fibrosis.

Table 1. Mean difference in MRI indices between groups

MRI indices	Control (Group 1)	Low-dose (Group 2)	High-dose (Group 3)	p	Post-hoc analysis*
RLE-3	2.84 ± 0.29	1.96 ± 0.23	1.87 ± 0.18	<0.001	1 vs 2, 1 vs 3
RLE-15	1.93 ± 0.34	1.67 ± 0.05	1.53 ± 0.29	<0.001	1 vs 3
iAUC-3	6.54 ± 0.51	5.49 ± 0.37	5.20 ± 0.36	<0.001	1 vs 2, 1 vs 3
iAUC-15	35.37 ± 3.07	28.25 ± 2.09	25.84 ± 2.92	<0.001	1 vs 2, 1 vs 3
Emax	3.03 ± 0.26	2.28 ± 0.23	2.12 ± 0.20	<0.001	1 vs 2, 1 vs 3

* Pairs with statistically significant difference in post-hoc analysis were present.

Table 2. Correlation between MRI indices and collagen area and between MRI indices and ICG-R15

MRI indices	Collagen area	95% CI	p	ICG-R15	95% CI	p
RLE-3	-0.80	-0.91 to -0.57	<0.001	-0.62	-0.82 to -0.27	0.002
RLE-15	-0.51	-0.77 to -0.12	0.015	-0.56	-0.80 to -0.18	0.006
iAUC-3	-0.78	-0.90 to -0.53	<0.001	-0.63	-0.83 to -0.28	0.002
iAUC-15	-0.81	-0.92 to -0.58	<0.001	-0.65	-0.84 to -0.31	0.001
Emax	-0.81	-0.92 to -0.59	<0.001	-0.58	-0.80 to -0.21	0.005

* Pairs with statistically significant difference in post-hoc analysis were present.

Figure 6. Gross specimen and gadoxetate-enhanced MRI images of the liver at 15 minutes

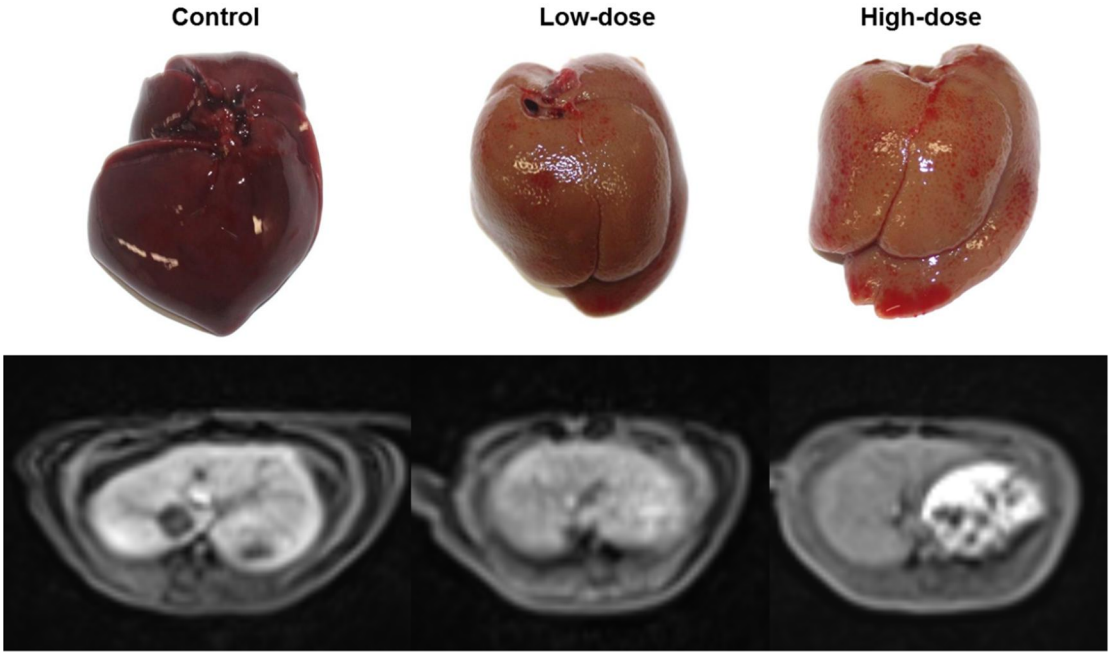

Figure 7. ROC curves and AUROC of MRI indices to diagnose liver fibrosis.

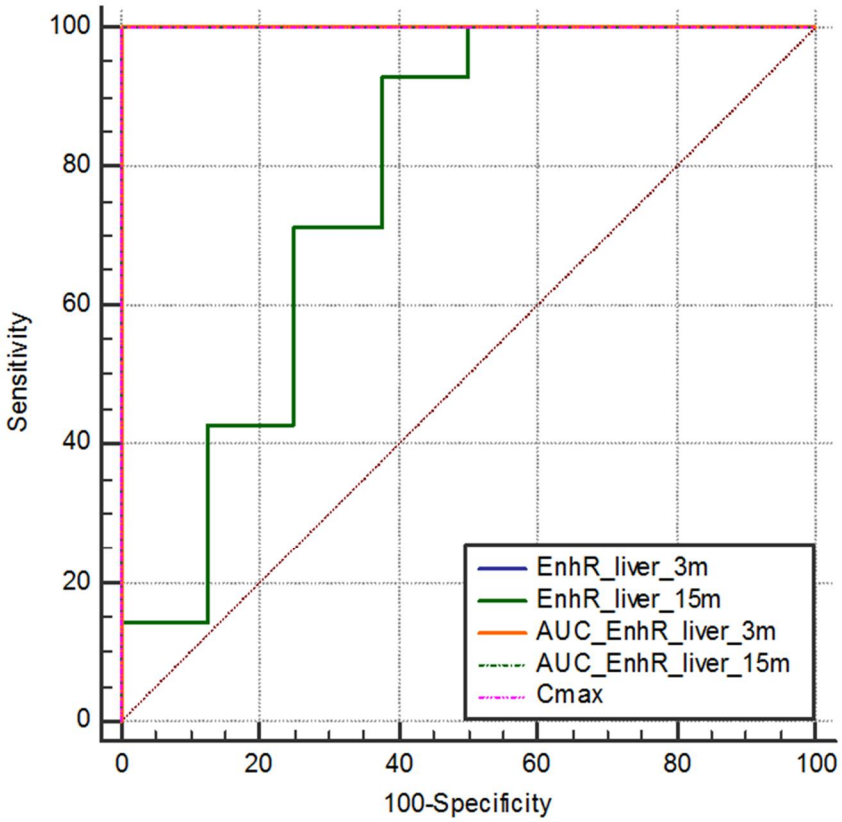

Variable	AUC	SE [a]	95% CI [b]
EnhR_liver_3m	1	0	0.846 to 1.000
EnhR_liver_15m	0.777	0.122	0.551 to 0.924
AUC_EnhR_liver_3m	1	0	0.846 to 1.000
AUC_EnhR_liver_15m	1	0	0.846 to 1.000
Cmax	1	0	0.846 to 1.000

DISCUSSION

In our preclinical study using liver fibrosis animal model, we demonstrated that the ultrasonographic SWE and gadoxetate-enhanced DCE-MRI are quite feasible to evaluate histopathologic liver fibrosis and physiologic liver function in non-invasive manner. Among the imaging parameters of SWE and DCE-MRI, the iAUC-15 might be the best index to evaluate both histopathologic liver fibrosis and physiologic liver function based on the highest correlation coefficients ($r = -0.81$ and -0.65, respectively).

The necessity to monitor the degree of liver fibrosis in a non-invasive and repeatable manner is increasing in the preclinical trial. However, still, histopathologic evaluation is considered the gold standard for quantification of liver fibrosis, which requires inevitably sacrificing the animal. Therefore, histopathologic evaluation after sacrificing the animal has a significant limitation that it provides only one time-point information per one animal (25). Liver biopsy might be possible in rats, however it also imposes significant risk of death, hemorrhage, and inflammation/infection. Furthermore, liver biopsy in rats generally obtains only small piece of tissue, limiting accurate evaluation (13). Therefore, imaging such as SWE and gadoxetate-enhanced MRI is gaining emphasis.

In both preclinical research and clinical practice, ultrasonography is much more convenient to perform, readily available, and less expensive compared to MRI. In addition, the ultrasonography is not invasive at all without necessity of intravenous catheter placement, while MRI has risks related with contrast agent injection. Cost of ultrasonography is also much lower than MRI. On the contrary, MRI has advantages that the accurate functional evaluation of liver function as well as detailed anatomic evaluation are possible. Therefore, we propose that combined use of SWE and MRI such as weekly SWE and monthly DCE-MRI can achieve non-invasive longitudinal follow-up as well as accurate evaluation of liver

fibrosis.

The ultrasonographic SWE can provide multiple time-point information along the time course without sacrificing animals and is generally very easy to perform in preclinical trial. However, our study revealed that the SWE in rats is highly dependent on operator's skill and experience. The variability of SWE results was greatly reduced in the second measurement session compared to the first session, implicating the learning or training effect of the operator. Therefore, if we standardize the method to perform SWE, the intra- and inter-operator variability might be reduced (26).

Indeed, in clinical practice, extensive researches have been performed to obtain accurate and reliable SWE data, which revealed that there are many technical factors such as measurement depth, ROI location, and number of measurement, which can a ect the results of US elastography (3). In our preclinical study, we standardized the SWE measurement method that measurement depth was at 1 cm below the left liver capsule, ROIs were placed in the areas of homogenous color on speed map in the left liver, and measurements were performed more than 8 times.

Despite these efforts, there were four outliers in the first measurement session. When we analyzed the outlier cases, the ROIs were placed when the speed maps showed heterogenous color map with several non-filling areas, which are indicative of invalid shear wave characteristics. Although liver fibrosis might not be uniform, measurement when there is visible homogeneity within ROIs may improve the artefactual or technical sources of variation (27).

In terms of measurement location, we measured in the left liver of the rats, because the left liver is the best location for sonic window. However, measurement in the left liver might be influenced by the probe compression against the liver (28). In general, liver stiffness

measured in the left lobe is higher than that in the right lobe (3). Our study also showed tendency that liver stiffness measurement results in the left liver are somewhat high. In our study, we placed the ultrasonographic probe very gently to avoid pressure.

Recently, the World Federation for Ultrasound in Medicine and Biology (WFUMB) guidelines recommended the consideration of the "mean" value of 4 measurements when using shear wave speed measurements (29). In our study, we performed 8 measurements per each rat and selected 4 measurements in the middle out of the 8 measurements. This approach seems to be better than performing 4 measurements, because it can remove outliers and reduce artefactual or technical sources of variation.

In our study, the test-retest repeatability of SWE measurement is generally good (within-subject CV 9.29%) when we measured the same rats twice with 3 days interval. This value was obtained in the ideal experiment setting including the same experienced operator, only 3 days interval, and trial-specific standardized protocol. Probably, the repeatability might be worse in the routine preclinical trial that include monitoring drug efficacy every several weeks or months. Training might be necessary for every sessions of measurement to minimize intra-operator variability.

Gadoxetate's uptake into the hepatocytes occurs via the organic anion transporter (OATP), and gadoxetate's biliary excretion occurs via the multidrug resistance-associated proteins (MRP) (30). These receptor-based influx and efflux mechanisms results in unique pharmacokinetic/pharmacodynamic characteristics, makes gadoxetate the most successful hepatocyte-specific MRI contrast agent, and enables us to evaluate liver function. In general, ICG clearance test and technetium-99m mebrofenin scintigraphy have been used for estimating liver function, because ICG and mebrofenin are substrates for OATP receptor of the hepatocytes and are excreted in the bile through MRP2 (30). Likewise, since gadoxetate is

also a substrate of OATP1B1 and OATP1B3 and is excreted through MRP2, gadoxetate-enhanced MRI can be used to estimate liver function. Liver fibrosis or cirrhosis causes a reduction of OATP and MRP2 level in the liver parenchyma, leads to a reduction of enhancement on gadoxetate-enhanced MRI. Therefore, the quantitative liver function evaluation is based on the degree of reduction of liver parenchymal enhancement on gadoxetate-enhanced MRI (12). Similarly, a recent preclinical study using a cirrhotic rat model also showed reduced liver parenchymal enhancement, attributed to slower hepatocyte uptake and rapid elimination due to decreased OATP1 activity and increased MRP2 activity (31).

The liver function estimation using gadoxetate-enhanced MRI can be categorized into three methods: (1) measurement of liver parenchymal SI on hepatobiliary phase (aka, RLE method), (2) MRI relaxometry such as T1 map or T2* map, and (3) DCE-MRI to utilize pharmacokinetic modelling (32-35). Regarding the measurement of the liver parenchymal SI, the absolute value of the SI differs across scans and MRI machines. Therefore, relative enhancement was calculated by subtracting the SI of the unenhanced images from the SI in the hepatobiliary phase and dividing the difference by the SI of the unenhanced images (i.e., RLE in our study). Sometimes, adjusting SI using internal tissue standards such as the spleen or muscles are utilized (32, 33, 36). The RLE method is very simple to use and does not require sophisticated software. However, its fundamental limitation is that the variability of enhancement level measured at only one time-point is high.

To overcome the limitation of RLE method, the DCE-MRI techniques has been proposed to estimate liver function based on measurements at many time-points (i.e., time-intensity curve). This approach enables us to use semi-quantitative analysis or sophisticated pharmacokinetic analysis based on a time-intensity curve of hepatic parenchyma and vessels.

As DCE-MRI techniques have been greatly advanced in the last decade, DCE-MRI methods have been increasingly utilized for liver function evaluation (35, 37).

In our study, we used the RLE method to measure RLE-3/RLE-15 and the DCE-MRI method to obtain semi-quantitative parameters such as iAUC-3, iAUC-15, and Emax. We did not use the hepatic extraction fraction (HEF) which requires a sophisticated modelling and special software. The reason why we did not use HEF is that it was very difficult to place ROIs on portal vein and hepatic vein of rats due to very small vessel size. Although HEF has been widely used in clinical studies, it might not be available for small animals such as rats and mice (35, 37). In our study, the semi-quantitative parameters of iAUC-3, iAUC-15, and Emax generally showed high correlation between ICG clearance and histopathologic fibrosis. Of the RLE method parameters, RLE-3 was good for liver fibrosis assessment, while RLE-15 was not. Of the all five MRI indices, the iAUC-15 might be the best index to estimate liver function based on the highest correlation with ICG-R15 ($r=-0.65$).

The liver function evaluation with gadoxetate-enhanced MR imaging has several advantages over traditional ICG test (12). The MRI can evaluate liver anatomy and liver function in localized hepatic abnormalities, which is more clinically relevant than a global assessment (38). ICG clearance is a method for global assessment of liver function. In addition, gadoxetate-enhanced MRI is non-invasive, whilst the ICG test requires repeated blood sampling which may cause very critical condition for small animals.

To incorporate gadoxetate-enhanced MRI in the preclinical trial and research for liver function estimation, standardization is a very important prerequisite. Various MRI machines and image acquisition techniques have been used, that may hamper reproducibility of MRI to estimate liver function (12). At least, in the same preclinical trial, we should use the same image acquisition and analysis method, i.e., trial-specific standardization (39).

CONCLUSION

In preclinical trial with animal liver fibrosis model, the ultrasonographic SWE and gadoxetate-enhanced DCE-MRI are quite feasible to evaluate histopathologic liver fibrosis and physiologic liver function in non-invasive manner. The SWE is more easy to use, non-invasive, and readily available than MRI. The MRI can access the liver function more accurately than SWE.

REFERENCES

1. Ramachandran P, Henderson NC. Antifibrotics in chronic liver disease: tractable targets and translational challenges. The lancet Gastroenterology & hepatology. 2016;1(4):328-40.
2. You MW, Kim KW, Pyo J, Huh J, Kim HJ, Lee SJ, et al. A Meta-analysis for the Diagnostic Performance of Transient Elastography for Clinically Significant Portal Hypertension. Ultrasound in medicine & biology. 2017;43(1):59-68.
3. Park SH, Kim SY, Suh CH, Lee SS, Kim KW, Lee SJ, et al. What we need to know when performing and interpreting US elastography. Clinical and molecular hepatology. 2016;22(3):406-14.
4. Ferraioli G, Tinelli C, Lissandrin R, Zicchetti M, Bernuzzi S, Salvaneschi L, et al. Ultrasound point shear wave elastography assessment of liver and spleen stiffness: effect of training on repeatability of measurements. European radiology. 2014;24(6):1283-9.
5. Amur S, LaVange L, Zineh I, Buckman-Garner S, Woodcock J. Biomarker Qualification: Toward a Multiple Stakeholder Framework for Biomarker Development, Regulatory Acceptance, and Utilization. Clinical pharmacology and therapeutics. 2015;98(1):34-46.
6. Alliance QIb. QIBA Profile Template-04-11-2016: Ultrasound Measurement of Shear Wave Speed for Estimation of Liver Fibrosis. Accessed at http://qibawiki.rsna.org/index.php/Ultrasound_SWS_Biomarker_Ctte2016.
7. Van Beers BE, Pastor CM, Hussain HK. Primovist, Eovist: what to expect? Journal of hepatology. 2012;57(2):421-9.
8. Tamada T, Ito K, Yoshida K, Kanki A, Higaki A, Tanimoto D, et al. Comparison of three different injection methods for arterial phase of Gd-EOB-DTPA enhanced MR imaging of the liver. European journal of radiology. 2011;80(3):e284-8.
9. Choi Y, Huh J, Woo DC, Kim KW. Use of gadoxetate disodium for functional MRI based

on its unique molecular mechanism. The British journal of radiology. 2016;89(1058):20150666.

10. Huh J, Kim KW, Kim J, Yu E. Pathology-MRI Correlation of Hepatocarcinogenesis: Recent Update. Journal of pathology and translational medicine. 2015;49(3):218-29.

11. Sung YS, Park B, Choi Y, Lim HS, Woo DC, Kim KW, et al. Dynamic contrast-enhanced MRI for oncology drug development. Journal of magnetic resonance imaging : JMRI. 2016;44(2):251-64.

12. Bae KE, Kim SY, Lee SS, Kim KW, Won HJ, Shin YM, et al. Assessment of hepatic function with Gd-EOB-DTPA-enhanced hepatic MRI. Digestive diseases (Basel, Switzerland). 2012;30(6):617-22.

13. Chen YW, Tsai MY, Pan HB, Tseng HH, Hung YT, Chou CP. Gadoxetic acid-enhanced MRI and sonoelastography: non-invasive assessments of chemoprevention of liver fibrosis in thioacetamide-induced rats with Sho-Saiko-To. PloS one. 2014;9(12):e114756.

14. Feier D, Balassy C, Bastati N, Stift J, Badea R, Ba-Ssalamah A. Liver fibrosis: histopathologic and biochemical influences on diagnostic efficacy of hepatobiliary contrast-enhanced MR imaging in staging. Radiology. 2013;269(2):460-8.

15. Zhang W, Kong X, Wang ZJ, Luo S, Huang W, Zhang LJ. Dynamic Contrast-Enhanced Magnetic Resonance Imaging with Gd-EOB-DTPA for the Evaluation of Liver Fibrosis Induced by Carbon Tetrachloride in Rats. PloS one. 2015;10(6):e0129621.

16. Bataller R, Gao B. Liver fibrosis in alcoholic liver disease. Seminars in liver disease. 2015;35(2):146-56.

17. Kang BK, Lee SS, Cheong H, Hong SM, Jang K, Lee MG. Shear Wave Elastography for Assessment of Steatohepatitis and Hepatic Fibrosis in Rat Models of Non-Alcoholic

Fatty Liver Disease. Ultrasound in medicine & biology. 2015;41(12):3205-15.

18. De Gasperi A, Mazza E, Prosperi M. Indocyanine green kinetics to assess liver function: Ready for a clinical dynamic assessment in major liver surgery? World J Hepatol. 2016;8(7):355-67.

19. Lee HB, Blaufox MD. Blood volume in the rat. Journal of nuclear medicine : official publication, Society of Nuclear Medicine. 1985;26(1):72-6.

20. Park JE, Han K, Sung YS, Chung MS, Koo HJ, Yoon HM, et al. Selection and Reporting of Statistical Methods to Assess Reliability of a Diagnostic Test: Conformity to Recommended Methods in a Peer-Reviewed Journal. Korean J Radiol. 2017;18(6):888-97.

21. Barnhart HX, Barboriak DP. Applications of the repeatability of quantitative imaging biomarkers: a review of statistical analysis of repeat data sets. Translational oncology. 2009;2(4):231-5.

22. Kessler LG, Barnhart HX, Buckler AJ, Choudhury KR, Kondratovich MV, Toledano A, et al. The emerging science of quantitative imaging biomarkers terminology and definitions for scientific studies and regulatory submissions. Statistical methods in medical research. 2015;24(1):9-26.

23. Krajewski KM, Nishino M, Franchetti Y, Ramaiya NH, Van den Abbeele AD, Choueiri TK. Intraobserver and interobserver variability in computed tomography size and attenuation measurements in patients with renal cell carcinoma receiving antiangiogenic therapy: implications for alternative response criteria. Cancer. 2014;120(5):711-21.

24. Baguley BC, Holdaway KM, Thomsen LL, Zhuang L, Zwi LJ. Inhibition of growth of colon 38 adenocarcinoma by vinblastine and colchicine: evidence for a vascular mechanism. Eur J Cancer. 1991;27(4):482-7.

25. Muller A, Machnik F, Zimmermann T, Schubert H. Thioacetamide-induced cirrhosis-

like liver lesions in rats--usefulness and reliability of this animal model. Experimental pathology. 1988;34(4):229-36.

26. Maruyama H, Kobayashi K, Kiyono S, Sekimoto T, Kanda T, Yokosuka O. Two-dimensional shear wave elastography with propagation-based reliability assessment for grading hepatic fibrosis and portal hypertension. Journal of hepato-biliary-pancreatic sciences. 2016;23(9):595-602.

27. Nadebaum DP, Nicoll AJ, Sood S, Gorelik A, Gibson RN. Variability of Liver Shear Wave Measurements Using a New Ultrasound Elastographic Technique. J Ultrasound Med. 2017.

28. Karlas T, Pfrepper C, Wiegand J, Wittekind C, Neuschulz M, Mössner J, et al. Acoustic radiation force impulse imaging (ARFI) for non-invasive detection of liver fibrosis: examination standards and evaluation of interlobe differences in healthy subjects and chronic liver disease. Scandinavian journal of gastroenterology. 2011;46(12):1458-67.

29. Ferraioli G, Filice C, Castera L, Choi BI, Sporea I, Wilson SR, et al. WFUMB guidelines and recommendations for clinical use of ultrasound elastography: Part 3: liver. Ultrasound in medicine & biology. 2015;41(5):1161-79.

30. de Graaf W, Hausler S, Heger M, van Ginhoven TM, van Cappellen G, Bennink RJ, et al. Transporters involved in the hepatic uptake of (99m)Tc-mebrofenin and indocyanine green. Journal of hepatology. 2011;54(4):738-45.

31. Tsuda N, Matsui O. Cirrhotic rat liver: reference to transporter activity and morphologic changes in bile canaliculi--gadoxetic acid-enhanced MR imaging. Radiology. 2010;256(3):767-73.

32. Tajima T, Takao H, Akai H, Kiryu S, Imamura H, Watanabe Y, et al. Relationship between liver function and liver signal intensity in hepatobiliary phase of gadolinium

ethoxybenzyl diethylenetriamine pentaacetic acid-enhanced magnetic resonance imaging. Journal of computer assisted tomography. 2010;34(3):362-6.

33. Yamada A, Hara T, Li F, Fujinaga Y, Ueda K, Kadoya M, et al. Quantitative evaluation of liver function with use of gadoxetate disodium-enhanced MR imaging. Radiology. 2011;260(3):727-33.

34. Katsube T, Okada M, Kumano S, Hori M, Imaoka I, Ishii K, et al. Estimation of liver function using T1 mapping on Gd-EOB-DTPA-enhanced magnetic resonance imaging. Investigative radiology. 2011;46(4):277-83.

35. Nilsson H, Blomqvist L, Douglas L, Nordell A, Janczewska I, Naslund E, et al. Gd-EOB-DTPA-enhanced MRI for the assessment of liver function and volume in liver cirrhosis. The British journal of radiology. 2013;86(1026):20120653.

36. Motosugi U, Ichikawa T, Sou H, Sano K, Tominaga L, Kitamura T, et al. Liver parenchymal enhancement of hepatocyte-phase images in Gd-EOB-DTPA-enhanced MR imaging: which biological markers of the liver function affect the enhancement? Journal of magnetic resonance imaging : JMRI. 2009;30(5):1042-6.

37. Ryeom HK, Kim SH, Kim JY, Kim HJ, Lee JM, Chang YM, et al. Quantitative evaluation of liver function with MRI Using Gd-EOB-DTPA. Korean J Radiol. 2004;5(4):231-9.

38. Nilsson H, Blomqvist L, Douglas L, Nordell A, Jacobsson H, Hagen K, et al. Dynamic gadoxetate-enhanced MRI for the assessment of total and segmental liver function and volume in primary sclerosing cholangitis. Journal of magnetic resonance imaging : JMRI. 2014;39(4):879-86.

39. Talakic E, Steiner J, Kalmar P, Lutfi A, Quehenberger F, Reiter U, et al. Gd-EOB-DTPA enhanced MRI of the liver: correlation of relative hepatic enhancement, relative

renal enhancement, and liver to kidneys enhancement ratio with serum hepatic enzyme levels and eGFR. European journal of radiology. 2014;83(4):607-11.

국문요약

연구 목적: 최근 간섬유화 및 만성간질환 치료약제 개발이 급증함에 따라 간섬유화 및 간기능 평가에 비침습적 이미징은 점차 큰 관심을 받고 있다. 초음파횡파탄성영상과 가도제테이트 역동조영증강 자기공명영상은 임상에서는 널리 사용되나 비임상시험에서는 아직 근거부족 등의 이유로 거의 사용되지 않고 있는 실정이다. 이에 본 연구에는 비임상시험에서 초음파횡파탄성영상과 가도제테이트 역동조영증강 자기공명영상의 효용성을 평가하고자 하였다.

연구방법: 총 31 마리 래트가 무작위로 3군으로 배정되었다 (고용량군, 저용량군, 비교군). 간섬유화는 티오아세타미드의 복강내 투여를 8주동안 함으로써 유도되었다. 티오아세타미드 용량은 고용량군에선 200mg, 저용량군에선 150mg를 투여하였다. 티오아세타미드 투여기간 이후에 초음파횡파탄성영상을 2일 간격으로 시행하였고 가도제테이트 역동조영증강 자기공명영상을 시행하였다. 초음파횡파탄성영상에서는 킬로파스칼을 지표로서 측정하였고, 자기공명영상에서는 5개 지표 (RLE-3, RLE-15, iAUC-3, iAUC-15, Emax)를 측정하였다. 각 이미징 지표와 병리결과 사이와 각 이미징 지표와 ICG-R15 결과 사이의 상관관계를 구했다. 또한 각 이미징 지표의 병리적 간섬유화를 올바르게 진단하는 진단능을 계산했다.

연구결과: 병리결과 동물모델은 모두 성공적으로 이루어졌다. 간조직의 콜라젠영역은 고용량군 (24.86 ± 4.55)에서 가장 높았고 저용량군(16.01 ± 3.25)과 비교군(6.27 ± 2.10)이 뒤따랐다. 상관관계는 iAUC-15, iAUC-3, RLE-3에서 유사하게 높았고 (-0.78 to -0.81) RLE-15(-0.51)과 킬로파스칼(-0.59)에선 낮았다. 자기공명영상 지표들과 ICG-R15 간기능검사 결과 사이의 상관관계는 iAUC-15 (-0.65)에서 가장 높았고, iAUC-3 (-0.63), RLE-3 (-0.62), Emax (-0.58), RLE-15 (-0.56) 순으로 낮아졌다. ROC 분석결과 간섬유화 진단능은 RLE-3, iAUC-3, iAUC-15, Emax는 모두 100% 였다 (AUROC 1.000). 반면 RLE-15의 진단능은 AUROC 0.777로서 낮았다.

결론: 간섬유화 동물모델을 이용한 비임상시험에서 초음파횡파탄성영상과 가도제테이트 역동조영증강 자기공명영상은 병리적 간섬유화 정도 평가 및 생리적 간기능 평가에 유용하게 활용될 수 있고 비침습적 특성으로 인해 더욱 유용하게 사용될 수 있다.

중심단어: 가도제테이트, 역동조영증강, 자기공명영상, 초음파횡파탄성영상, 평가